crystals

MDPI

Article

Transport Properties of the Two-Dimensional Hole Gas for H-Terminated Diamond with an Al_2O_3 Passivation Layer

Cui Yu [1], Chuangjie Zhou [1], Jianchao Guo [1], Zezhao He [1], Mengyu Ma [1], Hongxing Wang [2], Aimin Bu [1] and Zhihong Feng [1,*]

[1] National Key Laboratory of ASIC, Hebei Semiconductor Research Institute, Shijiazhuang 050051, China; yucui1@163.com (C.Y.); z19492010@163.com (C.Z.); guojian.chao@163.com (J.G.); hezezhao@sina.com (Z.H.); 17642082044@163.com (M.M.); 597664835@163.com (A.B.)

[2] School of Electronic and Information Engineering, Xi'an Jiaotong University, Xi'an 710049, China; hxwangcn@mail.xjtu.edu.cn

* Correspondence: ga917vv@163.com

Abstract: Diamonds are thought to be excellent candidates of next-generation semiconductor materials for high power and high frequency devices. A two-dimensional hole gas in a hydrogen-terminated diamond shows promising properties for microwave power devices. However, high sheet resistance and low carrier mobility are still limiting factors for the performance improvement of hydrogen-terminated diamond field effect transistors. In this work, the carrier scattering mechanisms of a two-dimensional hole gas in a hydrogen-terminated diamond are studied. Surface roughness scattering and ionic impurity scattering are found to be the dominant scattering sources. Impurity scattering enhancement was found for the samples after a high-temperature Al_2O_3 deposition process. This work gives some insight into the carrier transport of hydrogen-terminated diamonds and should be helpful for the development of diamond field effect transistors.

Keywords: diamond; carrier mobility; two-dimensional hole gas; carrier scattering mechanisms

check for updates

Citation: Yu, C.; Zhou, C.; Guo, J.; He, Z.; Ma, M.; Wang, H.; Bu, A.; Feng, Z. Transport Properties of the Two-Dimensional Hole Gas for H-Terminated Diamond with an Al_2O_3 Passivation Layer. *Crystals* **2022**, *12*, 390. https://doi.org/10.3390/cryst12030390

Academic Editors: Songang Peng, Yao Yao, Chaoyi Zhu and John Parthenios

Received: 14 February 2022
Accepted: 10 March 2022
Published: 14 March 2022

1. Introduction

Due to its high critical breakdown electric field, high carrier saturation drift velocity, high thermal conductivity, and high carrier mobility, diamonds have great application potential in high power and high frequency areas [1]. A hydrogen-terminated (H-terminated) diamond surface demonstrates a relatively high surface conductivity due to the forming of a two-dimensional hole gas (2DHG) by transfer doping from adsorbates/dielectric materials in contact with a H-terminated diamond surface. The electron transfer from the diamond to the adsorbates/dielectric materials and the holes accumulate in the subsurface of the H-terminated diamond [2,3]. The 2DHG shows a sheet density of 10^{12} to 10^{13} cm^{-2} and a carrier mobility of less than 200 $cm^2/(V{\cdot}s)$ [4–6].

H-terminated diamond field effect transistors (FETs) have obtained good direct current (DC) and radio frequency (RF) performances. A drain current density (I_{DSmax}) of 1.3 A/mm [7] and a maximum oscillation frequency (f_{max}) of 120 GHz [8] have been obtained for H-diamond FETs. Recently, the output power density was also improved and reached 3.8 W/mm at 1 GHz [9]. Output power densities at 2 GHz [10] and 10 GHz [11] were also reported. However, for high power and high frequency applications, the sheet resistance of the 2DHG is still at a high level and the carrier mobility is low, which leads to large parasitic resistance and limits the performance of H-terminated diamond FETs. Another issue is that, in the fabrication process of H-terminated diamond FETs, a gate dielectric, such as Al_2O_3 deposition, is needed, which is usually performed at a high temperature. The surface adsorbates would be broken during the high temperature process, which influences the electrical properties of the 2DHG of the H-terminated diamond. The atomic layer deposition (ALD) Al_2O_3 films are gate insulator and passivation films

for the p-type surface conduction of the H-terminated diamond surface. Many works have investigated the effects of Al_2O_3 passivation films [12–14]. Kawarada et al. [12,15] suggested that the surface adsorbates desorbed below 250 °C. There are defects in the ALD Al_2O_3 films, which introduce unoccupied levels above the valence band edge of Al_2O_3. The defects could accept the electrons transferring from the H-terminated diamond and be negatively charged. Ren et al. deposited an Al_2O_3 film at 300 °C and found that O impurity or Al vacancy defects existed in the ALD Al_2O_3 dielectric. Additionally, the ALD Al_2O_3 dielectric can work as an acceptor-like transfer doping material on the H-terminated diamond surface [16]. Liu et al. deposited Al_2O_3 at 120, 200, and 300 °C. They found that, when the deposition temperature of ALD Al_2O_3 was increased from 120 to 300 °C, the polarity of the fixed charges in the ALD Al_2O_3 dielectric changes from positive to negative [17]. The low carrier mobility of the 2DHG of the H-terminated diamond has been one of the limiting factors for the development of H-terminated diamond FETs. Some works have investigated the carrier scattering mechanism of the H-terminated diamond [18,19]. The deposition of Al_2O_3 may introduce an extra scattering source to the 2DHG of the H-terminated diamond and influence its electrical properties. However, to date, no report on the scattering mechanism analysis has been conducted for the Al_2O_3/H-terminated diamond structure.

In this work, the influence of Al_2O_3 deposition by a high-temperature ALD process on the transport properties of the 2DHG in a H-terminated diamond is investigated. The sheet resistance, carrier density, and mobility of H-diamond samples with and without Al_2O_3 were measured from 90 to 300 K by a Van der Pauw–Hall method. The temperature dependence of the mobility of the 2DHG is fitted considering four scattering mechanisms: ionic impurity (IM) scattering, acoustic phonon (AC) scattering, optical phonon (OP) scattering, and surface roughness (SR) scattering for the H-diamond samples with and without Al_2O_3 deposition.

2. Experiments

Three kinds of H-terminated diamond samples were prepared, as shown in Figure 1. The samples were prepared by the microwave plasma CVD (MPCVD, Seki diamond systems, Japan) technique. For the SC-Epitaxial H-termination samples, the samples were a single crystal diamond with a H-termination formed by a homoepitaxial growth process as stated in [20]. The microwave power was 1 kW, and growth temperature was 900 °C with a chamber pressure of 100 Torr. The CH_4/H_2 ratio was 1% with total flow of 500 sccm. For the SC-H plasma treatment and PC-H plasma treatment samples, the samples were treated by MPCVD in H_2 plasma [21]. The hydrogen plasma treatment was performed at a chamber pressure of 5 kPa and a temperature of 800 °C for 40 min. The SC-H plasma treatment samples were a single crystal diamond, and the PC-H plasma treatment samples were a polycrystalline diamond with a grain size of ~100 μm. The electrical properties of the H-terminated diamond samples were measured by the Van der Pauw–Hall method in the low temperature Hall measurement system from 90 K to 300 K.

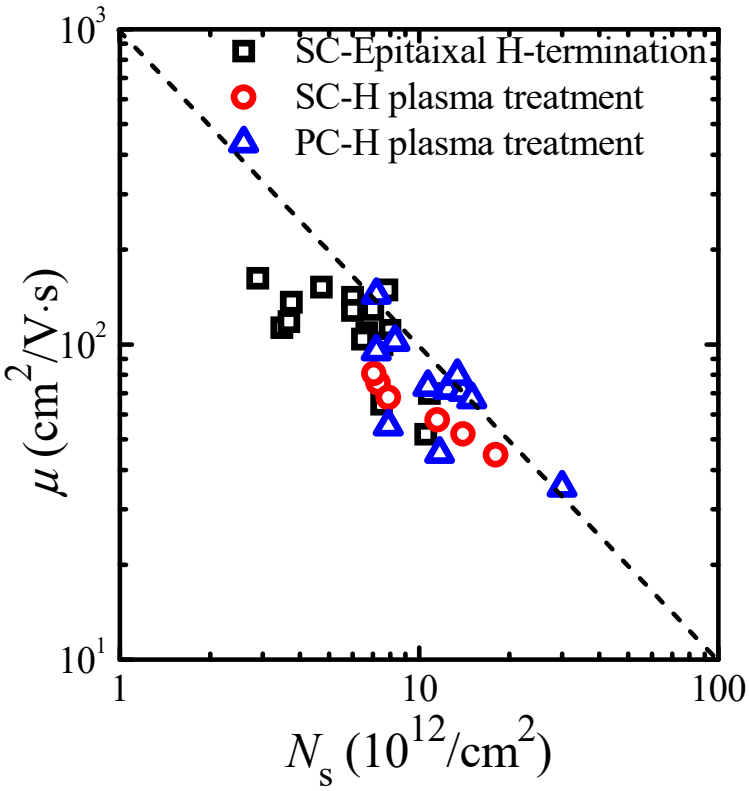

Figure 1. Relationship of carrier mobility μ vs. sheet density N_S at room temperature for the H-terminated diamond samples.

3. Results and Discussion

Figure 1 shows the relationship of carrier mobility μ vs. sheet density N_S at room temperature for the three kinds of H-terminated diamond samples. As shown in Figure 1, all the samples follow the $\mu \propto 1/N$s relationship, indicating the mobility of the 2DHG in the H-terminated diamond is limited by ionized impurity scattering [22]. The mobility values of the PC-H plasma treatment samples are comparable with the SC-Epitaxial H-termination samples and SC-H plasma treatment samples, showing that the grain boundary scattering is not dominant at this mobility level for the H-terminated diamond. This may be the reason why H-terminated diamond FETs on polycrystalline diamond samples show comparable or even better DC and RF properties than those on single crystal diamond samples [23].

To analyze the carrier transport mechanism of the 2DHG in H-terminated diamond, Van der Pauw–Hall measurements were performed. As listed in Table 1, five samples with (samples A, B, and C) and without (samples C and D) ALD Al_2O_3 deposition were studied. All the five samples are a single crystal diamond. The ALD processes were performed at 450 °C, 400 °C, and 300 °C for samples A, B, and C, respectively. From Table 1, it can be seen that the carrier mobility μ of the samples A, B, and C decreased after the Al_2O_3 deposition. The changes of the sheet density N_s of the samples are dependent on the deposition temperatures of the ALD Al_2O_3, as shown in Figure 2a and Table 1. For sample C with the ALD temperature of 300 °C, the sheet density Ns decreases. For sample B with the ALD temperature of 400 °C, the sheet density Ns shows a small decrease. Additionally, for sample A with the ALD temperature of 450 °C, the sheet density N_s increases. The adsorbates on the H-terminated diamond surface formed in the air desorbed from the surface during the heating process. Additionally, the ALD Al_2O_3 is the new transfer doping layer for the formation of the 2DHG of the H-terminated diamond. The different changes of sheet density N_s of the samples A, B, and C could be due to the different electron affinities of the ALD of Al_2O_3 deposited at different temperatures [24]. Hiraiwa et al. found that the Al_2O_3 electron affinity increases with the increasing of the Al_2O_3

deposition temperature. The high electron affinity of Al_2O_3 induces a high sheet density in the H-terminated diamond.

Table 1. Room temperature electrical properties of five H-terminated single crystal diamond samples with and without Al_2O_3 deposition.

Sample Name	Before Al_2O_3 Deposition			After Al_2O_3 Deposition			Al_2O_3 Deposition Temperature (°C)
	Rs (Ω/sq)	*Ns* (10^{12}/cm^2)	*μ* (cm^2/V·s)	*Rs* (Ω/sq)	*Ns* (10^{12}/cm^2)	*μ* (cm^2/V·s)	
A	8727	4.715	152	7360	6.18	137	450
B	9271	6.461	104	13,300	6	77.9	400
C	8332	7.512	99.7	11,500	5.37	101	300
D	7000	11.7	76.4		——		-
E	5380	14.3	80.9		——		-

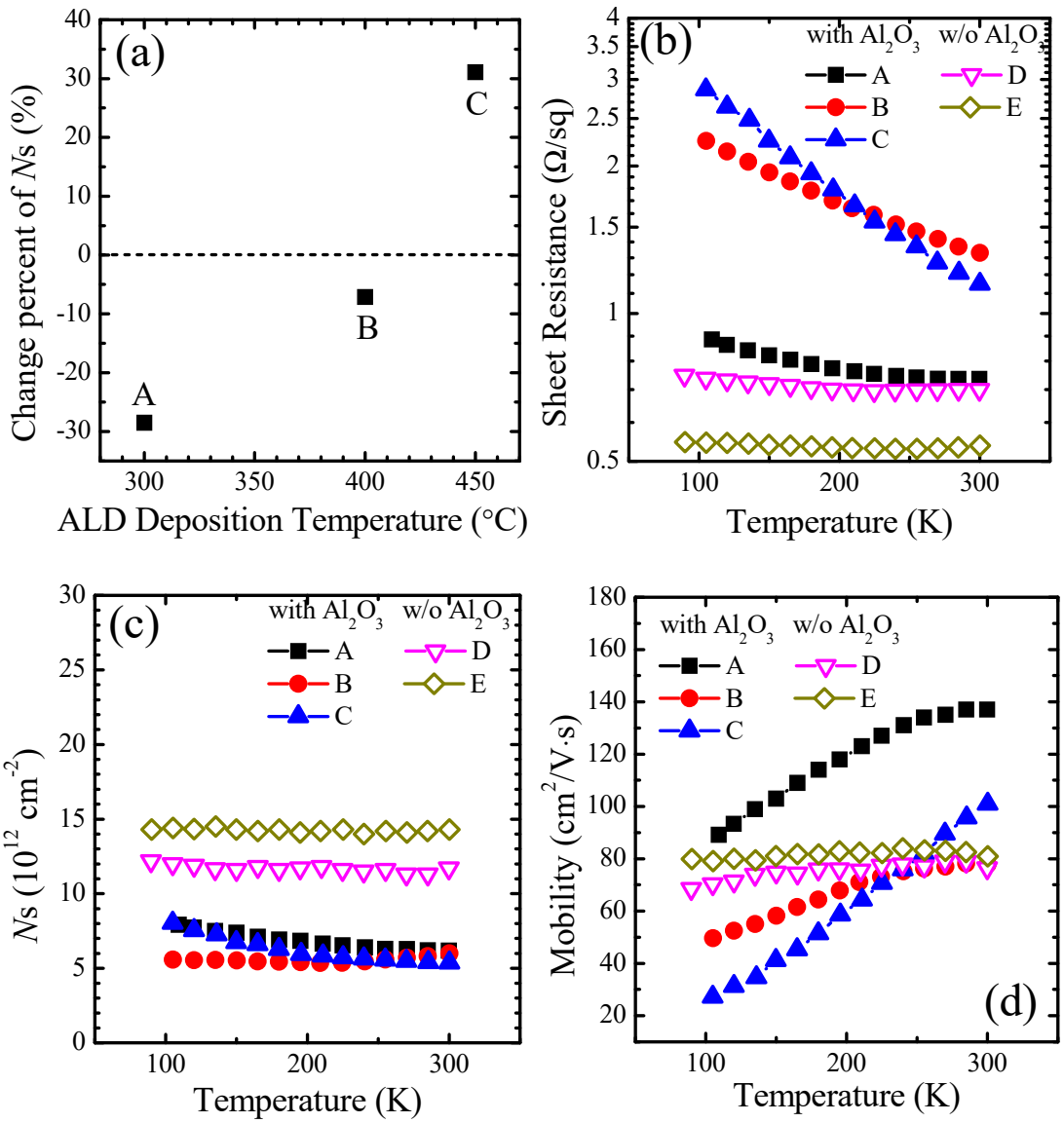

Figure 2. The electrical properties of the five H-terminated diamond samples with (samples A, B, and C) and without (samples D and E) ALD Al_2O_3. (**a**) Change of sheet density *N*s of the samples A, B, and C vs. performed temperatures of ALD processes. Temperature dependences of (**b**) sheet resistance, (**c**) sheet density, and (**d**) carrier mobility for the H-terminated diamond samples with and without ALD Al_2O_3.

Figure 2b shows the temperature dependences of the sheet resistance *Rs* of the H-terminated diamond samples with and without the ALD Al_2O_3. The sheet resistances of all the five samples decrease with temperature, which are due to the carrier mobility increases with temperature, as shown in Figure 2d. The sheet densities of the H-terminated diamond samples keep unchanged or slightly reduced with temperature, as shown in Figure 2c. The weak dependence of sheet density with temperature should be due to the electron affinity difference of the ALD Al_2O_3 and the H-terminated diamond is almost unchanged in the temperature range from 90 to 300 K. The carrier mobility of all the five samples increases with temperature. The carrier mobility of the H-terminated diamond samples with Al_2O_3 (samples A, B, and C) shows a stronger temperature dependence compared with those without (w/o) Al_2O_3 (samples D and E). The temperature dependence of the mobility of the 2DHG is fitted considering four scattering mechanisms to analyze the influences of Al_2O_3 deposition on the transport properties of the 2DHG in the H-terminated diamond.

The total relaxation time can be obtained by the Mathiessen rule:

$$\frac{1}{\tau} = \sum_n \frac{1}{\tau_n} \tag{1}$$

where τ_n is the momentum relaxation time corresponding to the n_{th} scattering mechanism. The mobility of the 2DHG of the H-terminated diamond can be obtained by the equation $\mu = e\tau/m_c^*$, where m_c^* is the conduction mass, and formulated as $m_c^* = (m_{lh}^{*3/2} + m_{hh}^{*3/2} + m_{so}^{*3/2})/(m_{lh}^{*1/2} + m_{hh}^{*1/2} + m_{so}^{*1/2})$ [25,26] with m_c^* = 0.444731 m_0. The quantities $m_{hh}{}^*$, $m_{lh}{}^*$, and $m_{so}{}^*$ are the heavy, light, and spin-orbit hole mass, respectively.

(1) Acoustic phonon (AC) scattering

Phonons are the quanta of the lattice vibrations of materials and introduce intrinsic scatterings to carriers. Due to different modes of vibrations, phonons can be divided into acoustic phonons and optical phonons. In this work, the relaxation time limited by the acoustic phonon was calculated following the formula for 2DEG [27]:

$$\frac{1}{\tau_{ac}} = \frac{3m_d^* b k_B T D_{ac}^2}{16\rho u_l^2 \hbar^3} \tag{2}$$

where ρ is the mass density, k_B is the Boltzmann constant, D_{ac} is the acoustic deformation potential, and u_l is the longitudinal acoustic phonons velocity. The parameter $b = \left[33\pi m_d^* e^2 p_{s2D}/\left(2\hbar^2\varepsilon_0\varepsilon_s\right)\right]^{1/3}$. In this paper, the acoustic deformation potential was considered as 8 eV. The density of state mass of diamond m_d^* was evaluated as $m_d^* = \left(m_{lh}^{*3/2} + m_{hh}^{*3/2} + m_{so}^{*3/2}\right)^{2/3}$ [28] and m_d^* = 0.907832 m_0.

(2) Optical phonon (OP) scattering

The Debye temperature is about 2240 K for a diamond, which is very high. If the optical phonons dominate the carrier scattering, an exponential drop in carrier mobility with temperature is expected for T < 600 K. The carrier mobility can be estimated by [29]:

$$\mu_{OP} = \frac{4\sqrt{2\pi}q\rho\hbar^2\sqrt{k\Theta}}{3D_0^2(m_d^*)^{3/2}m_c^*}\varphi(T) \tag{3}$$

where D_0 is the optical deformation potential. $\varphi(T)$ is a temperature-dependent function, which is in an exponential relationship and drops with temperature T below the Debye temperature.

(3) Ionic impurity (IM) scattering

Due to its deep impurity levels, the ionized impurity concentration is not a constant for diamond. This makes the ionic impurity scattering momentum relaxation time show a

strong temperature dependence. The classical expression for the ionized impurity scattering momentum relaxation time is the Brooks–Herring expression [30]:

$$\tau_{im} = \frac{16\sqrt{2m_c^*}\pi\varepsilon^2}{Z^2q^4N_I}(\ln(1+b) - b/(1+b))E^{3/2} \tag{4}$$

where $b = 8m_c^*L_D^2E/\hbar^2$ and ε is the dielectric constant of the medium. N_I is the ionized impurity concentration. Z is degree of ionization. L_D is the Debye length and E is the carrier energy. Assuming parabolic bands, by averaging over carrier momentum and neglecting the weak dependence of b on energy, the ionized impurity scattering limited relaxation time can be written as:

$$\tau_{im} = \frac{128\sqrt{2\pi m_c^*}\varepsilon^2(kT)^{\frac{3}{2}}}{Z^2q^4N_I(\ln(1+b') - b'/(1+b'))} \tag{5}$$

where $b' = 24m_c^*L_D^2kT/\hbar^2$.

(4) Surface roughness (SR) scattering

The relaxation time of SR is expressed including the screening by the 2DHG as [31]:

$$\frac{1}{\tau} = \frac{\Delta^2L^2e^4m_d^*}{2(\varepsilon_0\varepsilon_s)^2\hbar^3}\left(\frac{N_s}{2}\right)^2 \cdot \int_0^1 \frac{u^4\exp(-k_F^2L^2u^2)}{(u+G(q)q_{TF}/(2k_F))^2\sqrt{1-u^2}}du \tag{6}$$

where Δ is the root-mean-square roughness of surface and L is the correlation length. $u = q/2k_F$, which is a dimensionless parameter, with $q = 2k_F\sin(\theta/2)$, $\theta\in(0, \pi)$. θ is the angle between the initial and final wave vector.

Figure 3 shows the fitting results of the carrier mobility of the 2DHG with temperature for samples B and D. It can be seen that the surface roughness (SR) scattering and ionic impurity (IM) scattering are the dominant scattering sources in the measured temperature range. For sample B with Al_2O_3 deposition, the influence of IM scattering enhances, as shown in Figure 3a. This indicates that the adsorbates on the H-terminated diamond surface formed in the air desorbed from the surface during the heating process of the Al_2O_3 deposition. The ALD Al_2O_3 as the new transfer doping layer makes the concentration of the ionized impurity N_I increase. This is consistent with the results of Liu et al. [17]. They found that there were negative charges at the Al_2O_3/H-terminated diamond interface. They thought the unoccupied levels within the Al_2O_3 dielectric near the Al_2O_3/H-terminated diamond interface were the main sources of the negatively charged acceptors at the Al_2O_3/H-terminated diamond interface. The above results indicate that the initial stage of the ALD Al_2O_3 is especially important for the H-terminated diamond. The reduction of unoccupied levels in the Al_2O_3 near the Al_2O_3/H-terminated diamond interface will be beneficial for the carrier mobility improvement of the 2DHG in the H-terminated diamond.

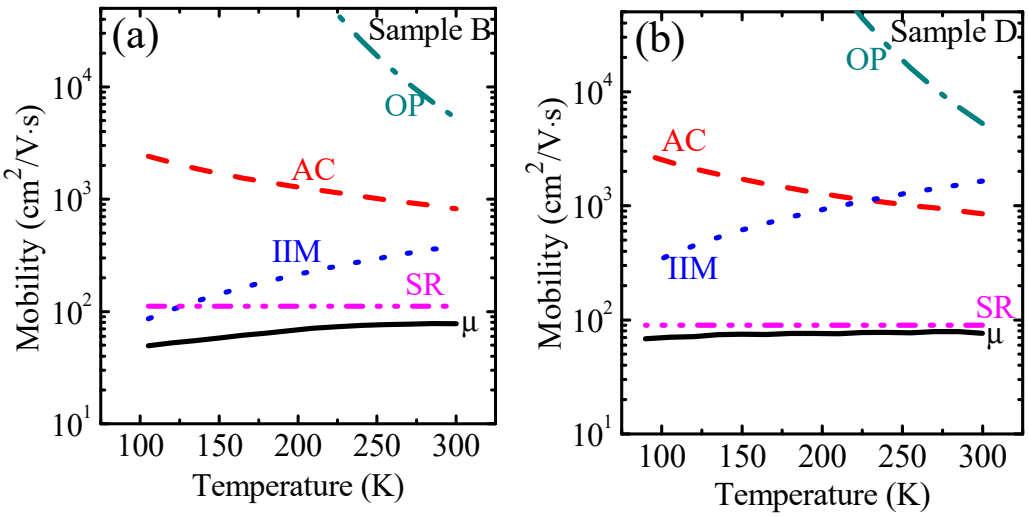

Figure 3. The fitting of carrier mobility as a function of temperature. (**a**) Sample B. (**b**) Sample D. AC represents the acoustic deformation potential scattering; OP is the nonpolar optical phonon scattering; SR is the interface roughness scattering; IM is the surface impurity scattering; and μ denotes the resulting 2DHG mobility covering the above four scattering mechanisms.

4. Conclusions

In summary, we studied the influence of Al_2O_3 deposition by a high-temperature atomic layer deposition process on the transport properties of the 2DHG in a H-terminated diamond. The temperature dependence of the mobility of the 2DHG is fitted considering four scattering mechanisms: ionic impurity scattering, acoustic phonon scattering, optical phonon scattering and surface roughness scattering. The surface roughness scattering and ionic impurity scattering are found to be the dominant scattering sources in the H-terminated diamond. Impurity scattering enhancement was found for the H-terminated diamond sample after the high-temperature atomic layer deposition Al_2O_3 process.

Author Contributions: Conceptualization, C.Y.; validation, Z.F., A.B.; formal analysis, C.Y.; investigation, C.Z., J.G., M.M. and H.W.; resources, C.Y.; data curation, C.Y. and Z.F.; writing—original draft preparation, C.Y.; writing—review and editing, C.Y.; visualization, C.Y.; supervision, Z.F. and A.B.; project administration, C.Y. and Z.H.; funding acquisition, C.Y. All authors have read and agreed to the published version of the manuscript.

Funding: National Key R&D Program of China, National Natural Science Foundation of the Hebei Province, and National Key Science and Technology Special Project.

Institutional Review Board Statement: Not applicable.

Informed Consent Statement: Not applicable.

Data Availability Statement: Not applicable.

Acknowledgments: This work was financially supported by the National Key R&D Program of China (Grant No. 2018YFE0125900), the National Natural Science Foundation of the Hebei Province (Grant No. F2019516002), and the National Key Science and Technology Special Project (Grant No. 2009ZYHW0015).

Conflicts of Interest: The authors declare no conflict of interest.

References

1. Wort, C.J.H.; Balmer, R.S. Diamond as an electronic material. *Mater. Today* **2008**, *11*, 22. [CrossRef]
2. Hui, J.L.; Pang, L.Y.S.; Molloy, A.B.; Jones, F.; Whitfield, M.D.; Foord, J.S.; Richard, B.J. Mechanisms of surface conductivity in thin film diamond: Application to high performance devices. *Carbon* **1999**, *37*, 801.
3. Kawarada, H.; Aoki, M.; Ito, M. Enhancement mode metal-semiconductor field effect transistors using homoepitaxial diamonds. *Appl. Phys. Lett.* **1994**, *65*, 1563. [CrossRef]

4. Williams, O.A.; Jackman, R.B. High growth rate MWPECVD of single crystal diamond. *Diam. Relat. Mater.* **2004**, *13*, 325. [CrossRef]
5. Looi, H.J.; Pang, L.Y.S.; Molloy, A.B.; Jones, F.; Foord, J.S.; Jackman, R.B. An insight into the mechanism of surface conductivity in thin film diamond. *Diam. Relat. Mater.* **1998**, *7*, 550. [CrossRef]
6. Jiang, N.; Ho, T. Electrical properties of surface conductive layers of homoepitaxial diamond films. *J. Appl. Phys.* **1999**, *85*, 8267. [CrossRef]
7. Hirama, K.; Sato, H.; Harada, Y.; Yamamoto, H.; Kasu, M. Diamond Field-Effect Transistors with 1.3 A/mm Drain Current Density by Al_2O_3 Passivation Layer. *Jpn. J. Appl. Phys.* **2012**, *51*, 090112.
8. Ueda, K.; Kasu, M.; Yamauchi, Y.; Makimoto, T.; Schwitters, M.; Twitchen, D.J.; Scarsbrook, G.A.; Coe, S.E. Diamond FET using high-quality polycrystalline diamond with f_T of 45 GHz and f_{max} of 120 GHz. *IEEE Electron. Device Lett.* **2006**, *27*, 57. [CrossRef]
9. Imanishi, S.; Horikawa, K.; Oi, N.; Okubo, S.; Kageura, T.; Hiraiwa, A.; Kawarada, H. 3.8 W/mm RF Power Density for ALD Al_2O_3-Based Two-Dimensional Hole Gas Diamond MOSFET Operating at Saturation Velocity. *IEEE Electron. Device Lett.* **2018**, *40*, 279–281. [CrossRef]
10. Zhou, C.J.; Wang, J.J.; Guo, J.C.; Yu, C.; He, Z.Z.; Liu, Q.B.; Gao, X.D.; Cai, S.J.; Feng, Z.H. Radiofrequency performance of hydrogenated diamond MOSFETs with alumina. *Appl. Phys. Lett.* **2019**, *114*, 063501. [CrossRef]
11. Yu, C.; Zhou, C.J.; Guo, J.C.; He, Z.Z.; Wang, H.X.; Cai, S.J.; Feng, Z.H. 650 mW/mm output power density of H-terminated polycrystalline diamond MISFET at 10 GHz. *Electron. Lett.* **2020**, *56*, 334–335. [CrossRef]
12. Kawarada, H.; Yamada, T.; Xu, D.; Kitabayashi, Y.; Shibata, M.; Matsumura, D.; Kobayashi, M.; Saito, T.; Kudo, T.; Inaba, M.; et al. Diamond MOSFETs using 2D Hole Gas with 1700V Breakdown Voltage. In Proceedings of the 28th ISPSD, Prague, Czech Republic, 12–16 June 2016; p. 483.
13. Ghasemi, M.H.; Abouei, V.; Moshtaghi, M.; Noghani, M.T. The effect of removing worn particles by ultrasonic cleaning on the wear characterization of LM13 alloy. *Surf. Eng. Appl. Electrochem.* **2015**, *51*, 382–388. [CrossRef]
14. Masafumi, K.; Ishii, H.; Shirai, Y.; Ohmi, T. High-corrosion-resistance Al_2O_3 passivation-film formation by selective oxidation on austenitic stainless steel containing Al. *J. Vac. Sci. Technol. A Vac. Surf. Film.* **2011**, *29*, 021002.
15. Hiraiwa, A.; Daicho, A.; Kurihara, S.; Yokoyama, Y.; Kawarada, H. Refractory two-dimensional hole gas on hydrogenated diamond surface. *J. Appl. Phys.* **2012**, *112*, 124504.
16. Ren, Z.; Lv, D.; Xu, J.; Zhang, J.; Zhang, J.; Su, K.; Zhang, C.; Hao, Y. High temperature (300 °C) ALD grown Al_2O_3 on hydrogen terminated diamond: Band offset and electrical properties of the MOSFETs. *Appl. Phys. Lett.* **2020**, *116*, 013503. [CrossRef]
17. Liu, J.W.; Oosato, H.; Da, B.; Koide, Y. Fixed charges investigation in Al_2O_3/hydrogenated-diamond metal-oxide semiconductor capacitors. *Appl. Phys. Lett.* **2020**, *117*, 163502. [CrossRef]
18. Sasama, Y.; Kageura, T.; Komatsu, K.; Moriyama, S.; Inoue, J.; Imura, M.; Watanabe, K.; Taniguchi, T.; Uchihashi, T.; Takahide, Y. Charge-carrier mobility in hydrogen-terminated diamond field-effect transistors. *J. Appl. Phys.* **2020**, *127*, 185707. [CrossRef]
19. Li, Y.; Zhang, J.F.; Liu, G.P.; Ren, Z.Y.; Zhang, J.C.; Hao, Y. Mobility of two-dimensional hole gas in H-terminated diamond. *Phys. Status Solidi (RRL)* **2018**, *12*, 1700401. [CrossRef]
20. Wang, J.J.; He, Z.Z.; Yu, C.; Song, X.B.; Wang, H.X.; Lin, F.; Feng, Z.H. Comparison of field-effect transistors on polycrystalline and single-crystal diamonds. *Diam. Relat. Mater.* **2016**, *70*, 114–117. [CrossRef]
21. Wang, J.J.; He, Z.Z.; Yu, C.; Song, X.B.; Xu, P.; Zhang, P.W.; Guo, H.; Liu, J.L.; Li, C.M.; Cai, S.J.; et al. Rapid deposition of polycrystalline diamond film by DC arc plasma jet technique and its RF MESFETs. *Diam. Relat. Mater.* **2014**, *43*, 43–48. [CrossRef]
22. Koizumi, S.; Nebel, C.; Nesladek, M. (Eds.) *Physics and Applications of CVD Diamond*; John Wiley & Sons: Hoboken, NJ, USA, 2008.
23. Camarchia, V.; Cappelluti, F.; Ghione, G.; Limiti, E.; Moran, D.A.J.; Pirola, M. An overview on recent developments in RF and microwave power H-terminated diamond MESFET technology. In Proceedings of the 2014 International Workshop on Integrated Nonlinear Microwave and Millimetre-Wave Circuits (INMMiC), Leuven, Belgium, 2–4 April 2014; IEEE: New York, NY, USA, 2014. ISBN 978-1-4799-3454-6/14/.
24. Hiraiwa, A.; Matsumura, D.; Kawarada, H. Effect of atomic layer deposition temperature on current conduction in Al_2O_3 films formed using H_2O oxidant. *J. Appl. Phys.* **2016**, *120*, 084504.
25. Tsukioka, K.; Okushi, H. Hall mobility and scattering mechanism of holes in boron-doped homoepitaxial chemical vapor deposition diamond thin films. *Jpn. J. Appl. Phys.* **2006**, *45*, 8571. [CrossRef]
26. Tsukioka, K. Scattering mechanisms of carriers in natural diamond. *Jpn. J. Appl. Phys.* **2001**, *40*, 3108. [CrossRef]
27. Davies, J.H. *The Physics of Low-Dimensional Semiconductors: An Introduction*; Cambridge University Press: Cambridge, UK, 1998; p. 365.
28. Pernot, J.; Volpe, P.N.; Omnès, F.; Muret, P.; Mortet, V.; Haenen, K.; Teraji, T. Hall hole mobility in boron-doped homoepitaxial diamond. *Phys. Rev. B* **2010**, *81*, 205203. [CrossRef]
29. Sussmann, R.S. *CVD Diamond for Electronic Devices and Sensors*; John Wiley & Sons, Ltd.: Hoboken, NJ, USA, 2009; ISBN 978-0-470-06532-7.
30. Brooks, H. *Advances in Electronics and Electron Physics*; Marton, L., Ed.; Academic Press: New York, NY, USA, 1955; p. 158.
31. Zanato, D.; Gokden, S.; Balkan, N.; Ridley, B.K.; Schaff, W.J. The effect of interface-roughness and dislocation scattering on low temperature mobility of 2D electron gas in GaN/AlGaN. *Semicond. Sci. Technol.* **2004**, *19*, 427. [CrossRef]